Published OnlineFirst September 17, 2019; DOI: 10.1158/0008-5472.CAN-18-3029

Tumor Biology and Immunology

Cancer Research

Chromosomal Instability and mTORC1 Activation through PTEN Loss Contribute to Proteotoxic Stress in Ovarian Carcinoma

M. Herman Chui[1,2,3], Sasha A. Doodnauth[1,4], Natalie Erdmann[1], Rodger E. Tiedemann[1,4], Fabrice Sircoulomb[1], Ronny Drapkin[5], Patricia Shaw[2], and Robert Rottapel[1,4,6,7,8]

Abstract

High-grade serous ovarian carcinoma commonly arises from fallopian tube secretory epithelium and is characterized by a high level of chromosomal instability. To model the acquisition of aneuploidy during early carcinogenesis, chromosome missegregation was induced in immortalized tubal epithelial cells, which proved acutely detrimental to cellular fitness. The phenotype was characterized by accumulation of misfolded proteins, activation of the unfolded protein response (UPR), decreased protein synthesis, and enhanced vulnerability to proteasome inhibition. However, chromosome missegregation also resulted in heightened transformation potential, assessed by colony formation in soft agar. Ovarian cancer cells retained intrinsic sensitivity to proteasome inhibitors under adherent culture conditions, but acquired resistance as spheroids (recapitulating their native configuration in ascites) by downregulating protein synthesis via mTORC1 suppression. Loss of PTEN drove constitutive mTORC1 activity, enhanced proteotoxic stress, as evidenced by UPR induction, and resensitized tumor spheroids to proteasome inhibition both *in vitro* and *in vivo*. In cohorts of primary ovarian carcinomas, mTORC1 and UPR signaling pathways were closely associated. These results implicate attenuation of protein synthesis as a protective mechanism in tumor spheroids, which may explain the overall poor response to bortezomib in clinical trials of patients with advanced ovarian cancer. However, patients with PTEN-deficient tumors may represent a subpopulation potentially amenable to treatment with proteasome inhibitors or other therapeutic agents that disrupt protein homeostasis.

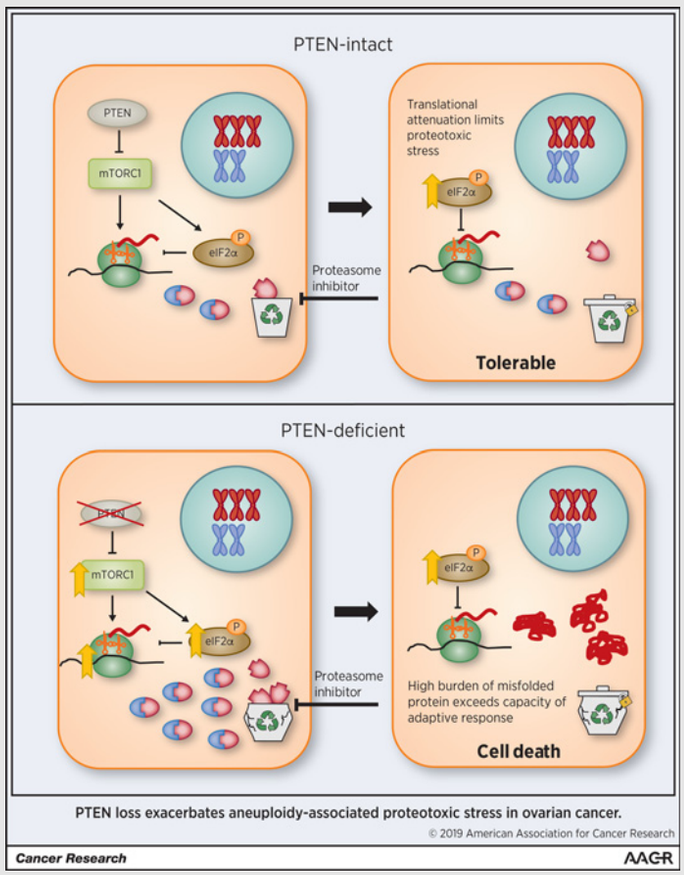

Significance: Chromosome instability and protein synthesis are important factors that determine the efficacy of proteotoxic stress-inducing agents, such as proteasome inhibitors, in the treatment of ovarian cancer.

Graphical Abstract: http://cancerres.aacrjournals.org/content/canres/79/21/5536/F1.large.jpg.

[1]Princess Margaret Cancer Centre, University Health Network, Toronto, Ontario, Canada. [2]Department of Laboratory Medicine and Pathobiology, University of Toronto, Toronto, Ontario, Canada. [3]Department of Pathology, Memorial Sloan Kettering Cancer Center, New York, New York. [4]Department of Medicine, University of Toronto, Toronto, Ontario, Canada. [5]Department of Obstetrics and Gynecology, Perelman School of Medicine, University of Pennsylvania, Philadelphia, Pennsylvania. [6]Department of Immunology, University of Toronto, Toronto, Ontario, Canada. [7]Department of Medical Biophysics, Faculty of Medicine, University of Toronto, Toronto, Ontario, Canada. [8]Division of Rheumatology, St. Michael's Hospital, Toronto, Ontario, Canada.

Note: Supplementary data for this article are available at Cancer Research Online (http://cancerres.aacrjournals.org/).

Corresponding Author: Dr. Robert Rottapel, Princess Margaret Cancer Research Tower, University Health Network, 101 College Street, Room 12-704, Toronto, ON M5G 1L7, Canada. Phone: 416-581-7852; E-mail: rottapel@gmail.com

Cancer Res 2019;79:5536–49

doi: 10.1158/0008-5472.CAN-18-3029

©2019 American Association for Cancer Research.

Downloaded from cancerres.aacrjournals.org on December 8, 2019. © 2019 American Association for Cancer Research.

Published OnlineFirst September 17, 2019; DOI: 10.1158/0008-5472.CAN-18-3029

Introduction

High-grade serous ovarian carcinoma (HGSOC) is the most common and most aggressive type of ovarian cancer (1). Large-scale sequencing efforts, including The Cancer Genome Atlas (TCGA; ref. 2), have revealed a complex genomic landscape, dominated by gene copy-number alterations, as well as gains and losses of chromosome arms or entire chromosomes. Extensive chromosomal disruption has been associated with poor prognosis (3), presumably due to the ability of genetically unstable cells to evolve resistance to chemotherapy.

Widely considered to be a driving force in the development and progression of cancer, chromosomal instability (CIN), when occurring in normal cells, can also compromise cellular viability and proliferation (4–9). Experimental insertion of a single chromosome caused mRNA transcripts to increase proportionally with gene dosage (9). Changes at the protein level were less pronounced and components of multimolecular complexes were maintained at stoichiometric levels, owing to degradation of excess protein subunits by autophagy (10) and the ubiquitin–proteasome system (9). The added burden on the protein degradation machinery renders aneuploid cells prone to aggregation of misfolded proteins (6, 7, 9, 10). Chromosome missegregation causes endoplasmic reticulum (ER) stress, with expansion of the ER and activation of the unfolded protein response (UPR; refs. 4, 11).

Histomorphologic analyses of surgically resected high-grade serous ovarian carcinomas have identified precursor lesions within the fallopian tube, pinpointing the secretory epithelial cell (fallopian tube secretory epithelial cell, FTSEC) as a likely cell of origin (1, 12). Ultrastructural studies have identified abundant rough ER and well-developed Golgi complexes and presence of secretory vesicles in FTSECs—features maintained in the malignant state (13). High levels of protein synthesis in professional secretory cells render them especially dependent on protein quality control pathways. This is paradigmatically exemplified by the efficacy of the proteasome inhibitor, bortezomib in the treatment of multiple myeloma due to uncontrolled synthesis of immunoglobulins (14).

In light of these findings, we hypothesize that the genomic complexity of HGSOC, coupled with their derivation from secretory epithelial cells, renders these tumor cells poised for cell death from agents that exacerbate proteotoxic stress. However, in early-phase clinical trials, only a small minority of ovarian cancer patients achieved clinical benefit from bortezomib (15). The factors affecting treatment response are unknown.

To gain insight into the interplay between chromosomal disruption, proteostasis, and sensitivity to proteasome inhibition, we modeled the early events in the pathogenesis of HGSOC by experimentally inducing chromosome missegregation in immortalized, nontumorigenic FTSEC cell lines. We observed that CIN/aneuploidy caused ER stress, which engendered selective vulnerability to proteasome inhibition. Moreover, genetic depletion of PTEN was associated with increased protein synthetic rates, which exacerbated proteotoxic stress and sensitized cells to proteasome inhibition.

Materials and Methods

Cell lines and culture

FTSEC cell lines (FT194 and FT246) were obtained from Dr. R. Drapkin, University of Pennsylvania, Philadelphia, PA. Ovarian cancer cell lines were obtained from Dr. A.M. Mes-Masson, University of Montreal, Montreal, Quebec, Canada (TOV1946, TOV2223, and COV318), Dr. J. Brenton, University of Cambridge, Cambridge, United Kingdom (PEO1), and ATCC (OVCAR3, OVCAR8, SKOV3, A2780, and TOV21G). All cell lines were authenticated by STR profiling and tested to rule out *Mycoplasma* contamination at the time of receipt and periodically thereafter. Experiments using cell lines were performed within 9 passages after thawing from frozen stocks.

Cell lines were cultured in OSE (Wisent) supplemented with 10% fetal bovine serum (FBS, Gibco), 100 U/mL penicillin and 100 μg/mL streptomycin (Wisent). For culturing spheroids, cells were seeded to 96-well ultralow attachment cluster plates (Corning) at a density of 5,000 cells per well. For protein isolation from spheroids, cells were seeded at 5×10^5 cells per well of a 6-well plate precoated with poly-2-hydroxyethyl methacrylate (polyHEMA). Cells were cultured for 4 days in suspension to form spheroids for all experiments, unless otherwise specified. $TSC2^{+/+}$ and $TSC2^{-/-}$ MEFs were obtained from Dr. V. Stambolic, Princess Margaret Cancer Center, and were cultured in DMEM (Gibco) supplemented with 10% FBS (Gibco).

Primary short-term cultures and tumor specimens

Tumor spheroids were isolated directly from ascites fluid by centrifugation at 300 × *g* for 15 minutes, resuspended in OSE media with 5% FBS and seeded onto 15-cm cell culture dishes (Corning). After 24 hours, to allow mesothelial cells to attach to the plate, tumor spheroids in suspension were collected by centrifugation, washed with PBS, and lysed with 2× Laemmli sample buffer for protein extraction or fixed in 4% paraformaldehyde for 30 minutes and embedded in Histogel for subsequent paraffin embedding and processing for immunohistochemical staining. To establish adherent monolayer cultures, mesothelial cells and fibroblasts were removed by differential trypsinization, followed by the addition of fresh medium and incubation for at least 24 hours; the process was repeated until over 90% of remaining cells were tumor cells. The cells were then collected by scraping and centrifugation and processed as described for spheroids. Extracted DNA was analyzed for hotspot mutations in exons 9 and 20 of the *PIK3CA* gene, as previously described (16).

Tissue microarrays containing 128 ovarian carcinomas [62 (48.4%) serous, 37 (28.9%) endometrioid, 12 (9.4%) clear cell, 11 (8.6%) mucinous, 6 (4.7%) not otherwise specified] were constructed using deidentified samples from patients who underwent primary surgical resection at the University Health Network. Each case was represented by two or three cores.

Lentiviral transduction

Human pLKO.1 lentiviral shRNA constructs were obtained from The RNAi Consortium: *PTEN* shRNA#1: TRCN0000028991 and shRNA#2: TRCN0000002748. The pLVX-ZsGreen-mODC-IRES-mCherry construct (17) was a gift of Dr. G. Luker (University of Michigan, Ann Arbor, MI). Lentivirus production and transduction were performed as previously described (18).

Cell treatments

GSK923295, AZ3146, and bortezomib were from Selleckchem; cycloheximide was from Sigma-Aldrich. To induce chromosome missegregation, cells were treated with GSK923295

Downloaded from cancerres.aacrjournals.org on December 8, 2019. © 2019 American Association for Cancer Research.

Published OnlineFirst September 17, 2019; DOI: 10.1158/0008-5472.CAN-18-3029

(50 nmol/L) and AZ3146 (2 μmol/l) for 96 hours, with replating and replacement of drug-containing medium at 48 hours, to ensure cells remain in logarithmic growth phase. To assess bortezomib sensitivity, at the 96-hour time point, cells were seeded into triplicate wells of a 96-well plate in drug-free medium, allowed to adhere overnight, and treated at various concentrations of bortezomib or vehicle control (DMSO) for 48 hours.

To derive dose–response curves across a panel of cell lines, 5,000 cells were seeded per well in 96-well plates, allowed to adhere overnight, and treated with 2-fold dilutions from 160 to 2.5 nmol/L of bortezomib, alongside DMSO control, for 48 hours. For cells grown as monolayer adherent cultures, viability was determined by the CellTiter-Glo Luminescent Cell Viability Assay (Promega), as per the manufacturer's protocol. For spheroids, viability was determined by the CellTiter-Glo 3D Cell Viability Assay. The CyQUANT assay (Thermo Fisher) was used as an orthogonal method to assess cell viability, by quantification of total DNA content, and was performed following the manufacturer's protocol.

G-band karyotyping

Cells at 70% confluence were harvested using 0.1 μg/mL colcemid treatment (Life Technologies, Inc.) for 2 to 4 hours, hypotonic treatment with 0.075 m KCl, and fixed in 3:1 methanol:acetic acid. G-banding analysis was performed using standard methods. Karyotypes were designated according to the International System for Cytogenetic Nomenclature.

Fluorescent *in situ* hybridization

Cytospin slides were fixed in ice-cold 3:1 methanol/acetic acid, air-dried, incubated in 2× SSC pH7.0 10 minutes at 37°C, 0.005% pepsin in 0.01 N HCl 10 minutes at 37°C, washed 1× PBS 3 minutes, fixed in 1% formaldehyde/50 mmol/L $MgCl_2$ solution 5 minutes, washed 1× PBS 3 minutes, dehydrated in a series of ethanol washes, denatured in 70% formamide/1× SSC pH5.3 5 minutes at 73°C, and hybridized with fluorescent *in situ* hybridization (FISH) probes overnight at 37°C with red CEP8 (D8Z2) and green CEP17 (D17Z1) α-satellite probes (Cytocell Aquarius). Hybridized slides were washed in 0.4× SSC pH7.0/0.3% NP-40 2 minutes at 73°C, 2× SSC pH7.0/0.1% NP-40 1 minute at room temperature and mounted in a 1:7 mix of Vectashield mounting medium with/without DAPI (Vector Laboratories). Images were acquired and analyzed on a BioView Duet automated scanning system (BioView Ltd). Two hundred fifty cells were scored for each sample.

Immunofluorescence, Thioflavin T staining, and microscopy

Cells were grown on glass coverslips and fixed in 4% paraformaldehyde for 30 minutes, washed with PBS, permeabilized with 0.1% Triton-X for 10 minutes, followed by PBS wash, and blocking with goat serum for 1 hour. Incubation with primary antibody occurred overnight at 4°C, followed by 3 washes of PBS, 1-hour-incubation with secondary antibody, and another 3 washes of PBS. Coverslips were then mounted onto glass slides using ProLong Gold Antifade Mountant (Thermo Fisher) and the edges were sealed with nail polish. For Thioflavin T staining, cells were fixed in ice-cold methanol for 15 minutes. After washing with PBS, cells were incubated in the dark with 5 μmol/L Thioflavin T (Sigma-Aldrich) dissolved in PBS for 1 hour, followed by 3 washes of PBS.

Immunofluorescence data of mitotic figures were collected using a laser-scanning confocal system with a Leica DMI6000 microscope system using a 100× (NA 1.4) oil immersion objective. Images were acquired using HyD detector controlled using Leica LAS software (Leica). All other imaging data were collected using a spinning-disk confocal system (Quorum Technologies) with an Axiovert 200 M microscope (Carl Zeiss, Inc.) with 25× (NA 1.0) water immersion or 63× (NA 1.4) oil immersion objectives. Images were acquired using a back-thinned, electron-multiplied camera (model C9100-13 ImagEM; Hamamatsu Photonics) controlled using Volocity software, version 6.0.1 (PerkinElmer).

Homopropargylglycine incorporation assays

Cells were preincubated in methionine-free media for 15 minutes, followed by incubation in the same media in the presence of homopropargylglycine (HPG, 50 μmol/L; Thermo Fisher). For cell lysates, after 2 hours of metabolic labeling, cells were washed with PBS and lysed in RIPA buffer with Halt Protease Inhibitor cocktail (Thermo Scientific) and incubated at 4°C for 30 minutes. The Click-iT Protein Reaction Buffer Kit (Thermo Fisher) was used to perform a click chemistry reaction linking biotin-PEG3-azide (Sigma-Aldrich) to HPG-incorporated proteins, as per the manufacturer's instructions. Methanol/chloroform precipitated protein was solubilized in 2× sample buffer, subjected to SDS-PAGE, membrane transfer, blocking with 5% BSA, incubation in streptavidin-HRP (1:2000; Cell Signaling Technology), wash steps with TBST, and chemiluminescence detection. SDS-PAGE gels were also stained with Coomassie-Blue to visualize total protein.

Protein extraction and Western blotting

For preparation of detergent-soluble and insoluble fractions, cells were lysed in 1% Triton-X lysis buffer. After centrifugation for 15 minutes at 16,800 ×*g*, the soluble fraction was saved separately, and insoluble pellets were solubilized in 2× Laemmli sample buffer. For all other cell lysates, unless otherwise specified, cells were washed with ice-cold PBS and scraped directly into sample buffer and denatured at 95% for 5 minutes. Protein quantitation was performed using the Pierce 660 nm Protein Assay (Thermo Fisher), as per the manufacturer's instructions. SDS-PAGE and immunoblotting were performed as previously described (18).

Immunohistochemistry

Immunohistochemistry was performed using the Ventana Discovery XT and the Ventana Benchmark XT automated systems (Ventana Medical Systems), with primary antibodies at the following dilutions: p-S6 (1:400), PTEN (1:100), and p-eIF2α (1:100).

Scoring of tissue microarrays was performed by a board-certified pathologist (M.H. Chui). PTEN staining was classified dichotomously as intact (intensity ranging from weak to strong) or negative (complete loss of staining). The H-score was used to quantify p-eIF2α cytoplasmic staining, representing the weighted average of the proportion of cells at each staining intensity level: [1 × (% cells weak staining) + 2 × (% cells intermediate staining) + 3 × (% cells strong staining)].

Antibodies

Primary antibodies used for Western blotting and immunofluorescence are summarized in Supplementary Table S1. HRP-

Downloaded from cancerres.aacrjournals.org on December 8, 2019. © 2019 American Association for Cancer Research.

Published OnlineFirst September 17, 2019; DOI: 10.1158/0008-5472.CAN-18-3029

conjugated anti-mouse or anti-rabbit secondary antibodies were from GE Healthcare.

HGSOC transcriptomic data analysis

Preprocessed RNA-seq data from 6 normal fallopian tube samples were obtained from Dr. D. Bowtell. Details of this data set are described elsewhere (19). FASTQ files from the TCGA HGSOC RNA-seq data set were downloaded from cBioPortal. Transcript abundance was determined using Cufflinks 1.3.0 in fragment per kilobase per million reads (FPKM) and $\log_2$ transformed. Genes with high expression variability (MAD>1) in fallopian tube samples and genes not expressed ($\log_2$ FPKM < -1) in all samples (normal and tumor) were removed. Gene expression for each sample in each tumor was centered using median expression in all 6 normal samples. Median-centered expression values were loaded on the ssGSEA projection module from GenePattern (20) using the Hallmarks library with default options.

Flow cytometry

For ploidy analysis, cells were trypsinized, washed in PBS, fixed in ice-cold 70% ethanol overnight and resuspended in PBS containing 10 μg/mL RNase A and 20 μg/mL propidium iodide. To assess proliferation, cells were incubated for 2 hours in media containing 10 μg/mL BrdU, trypsinized, washed in PBS, and fixed in ice-cold 70% ethanol overnight. Fixed cells were then treated for 30 minutes with 2 N HCl, rinsed with PBS, blocked with 5% BSA with 0.2% Triton-X, followed by incubation with FITC-conjugated anti-BrdU antibody for 1 hour. Cells were washed with PBS twice and resuspended in PBS containing 10 μg/mL RNase A and 20 μg/mL propidium iodide. For apoptosis assays, cells were trypsinized, washed in ice-cold PBS, and resuspended in staining media (HBSS, 2% FBS, 2.5 mmol/L $CaCl_2$). Cells were transferred to polystyrene tubes, and stained with 100 μg/mL propidium iodide and 5 μL Annexin V–FITC (BD Pharmingen) for 15 minutes at room temperature protected from light. Cells were resuspended in 400 μL staining media. For all FACS analysis, fluorescence was measured using a Becton-Dickinson LSRII flow cytometer. FCS 3.0 files were exported and analyzed using FlowJo version 9.3.

Xenograft studies

TOV1946 cells stably transduced with the bicistronic lentiviral vector PKG-GFP-IRES-luc (TOV1946^{Luc}) were transduced with shRNA constructs targeting PTEN or GFP. Following 48-hour puromycin selection, 1.0×10^7 tumor cells in 200 μL equal volume mixture of growth-factor reduced Matrigel (BD 354230) and OSE medium were injected into the intraperitoneal cavity of 6-week-old immunodeficient NOD/SCID/IL2R$\gamma^{-/-}$ (NSG) mice (5 mice per condition). Tumor growth was monitored by injecting 10 μL of D-Luciferin per gram body weight from a stock of 15 mg/mL in PBS and bioluminescence was imaged using the Xenogen IVIS Spectrum Imaging System (PerkinElmer) in animals anesthetized with 2% isoflurane. Bioluminescence was quantified using the IVIS Live Image software (Caliper Life Sciences). Mice were sacrificed when moribund or upon recommendation by the research facility veterinarian.

Statistical analysis

Group comparisons were made by *t* test or ANOVA (with Bonferroni correction) for continuous data and Mann–Whitney test for ordinal (immunostain scoring) data. All statistical tests were two-tailed.

Study approval

All work with patient materials has been approved by the University Health Network Research Ethics Board, Toronto, Ontario. Written informed consent for collection of tissues for research was obtained from patients. All mouse experiments were approved by the University Health Network Animal Research Council.

Results

Chromosome missegregation in fallopian tube secretory epithelial cells is detrimental to cellular fitness, but enhances transformation potential

To study the phenotypic effects of CIN in fallopian tube epithelium, we induced chromosome missegregation in immortalized nontumorigenic FTSEC cell lines, FT194 and FT246 (21), showing "near-diploid" karyotypes (Supplementary Fig. S1A). During mitosis, the kinesin-like motor protein CENP-E aids in chromosome alignment at the metaphase plate, by mediating proper attachment of microtubules to the kinetochores of chromosomes (22). Inhibition of CENP-E leads to chromosome misalignment, triggering mitotic arrest through activation of the spindle assembly checkpoint (SAC). Therefore, concomitant suppression of CENP-E function and the SAC enables mitosis to proceed despite chromosome misalignment, resulting in unequal partitioning of chromosomes to daughter cells (4, 23).

Cells were treated with GSK923295, a specific inhibitor against CENP-E, with or without AZ3146, an inhibitor of the SAC kinase, Mps1. Immunofluorescence performed 24 hours after the addition of GSK923295 (CENP-E_i) demonstrated accumulation of mitotic cells in metaphase (Supplementary Fig. S1B). Most cells demonstrated several chromosomes positioned at the spindle poles (i.e., "polar chromosomes"; ref. 23), as expected from failure of CENP-E to bring chromosomes to the equatorial plate (Fig. 1A). Cotreatment with AZ3146 (Mps1_i + CENP-E_i) partially alleviated the metaphase arrest, with identifiable mitotic figures progressing through anaphase and telophase. Lagging chromosomes were frequently observed during anaphase in Mps1_i + CENP-E_i–treated cells and multipolar mitoses were more prevalent. Consistent with previous work showing that lagging chromosomes frequently incur damage during cytokinesis (24, 25), we also observed a time-dependent increase in levels of γH2AX, a marker of DNA double-strand breaks, in cells treated with Mps1_i + CENP-E_i (Supplementary Fig. S1C).

Interphase cells exhibited striking changes in nuclear morphology, with increased pleomorphism, multinucleation, and micronuclei. Ploidy distribution was determined by flow cytometry (FACS), which displayed marked broadening of the peaks, consistent with heterogeneity of DNA content, and the presence of occasional cells with ploidy exceeding 4N (Fig. 1B). FISH, using chromosome-specific centromeric α-satellite DNA probes for chromosomes 8 and 17, confirmed the emergence of karyotypic heterogeneity after chromosome missegregation (Fig. 1C; Supplementary Fig. S1D). Consistent with the detrimental effect of aneuploidy on cellular fitness, cells treated with Mps1_i + CENP-E_i, demonstrated impaired cell growth

Downloaded from cancerres.aacrjournals.org on December 8, 2019. © 2019 American Association for Cancer Research.

Published OnlineFirst September 17, 2019; DOI: 10.1158/0008-5472.CAN-18-3029

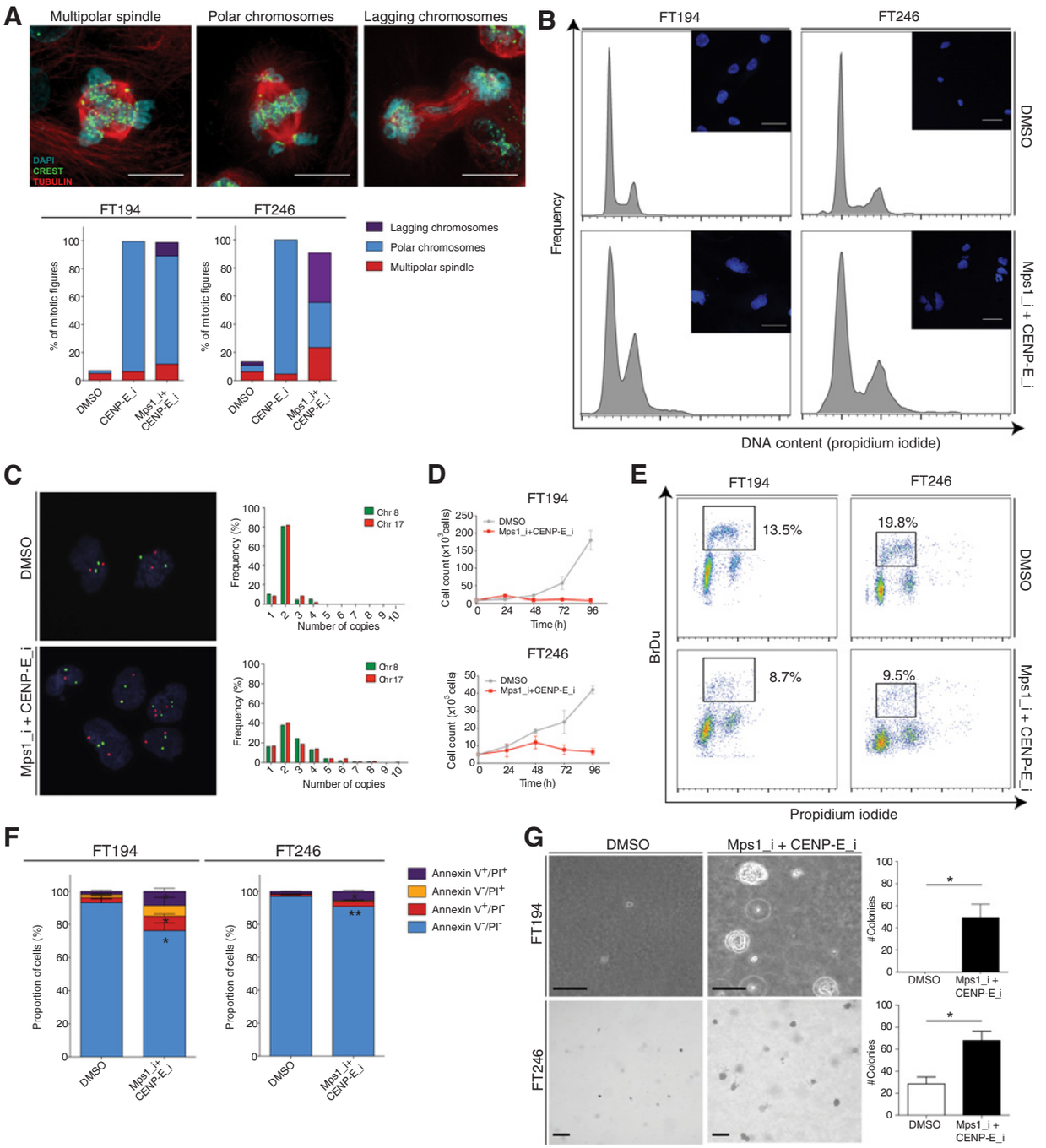

Figure 1.

Chromosome missegregation in FTSECs is associated with growth defect, but increased transformation potential. **A,** Immunofluorescence on fixed FT194 and FT246 cells treated with DMSO, CENP-E inhibitor (GSK923295, 50 nmol/L) alone or combined with Mps1 inhibitor (AZ3146, 2 μmol/L) for 24 hours. At least 50 mitotic figures (in metaphase or anaphase) were analyzed per condition. Scale bar, 10 μm. **B,** FTSEC cells were treated with Mps1 and CENP-E inhibitors combined or vehicle for 72 hours, and DNA content was analyzed by flow cytometry. The inset shows representative microscopic images of DAPI-stained nuclei. **C,** Interphase FISH using centromeric probes against chromosomes 8 and 17 (250 cells quantified per condition) in FT194 cells. **D,** Cells were plated at low density, treated with inhibitors or vehicle, and cell counts were performed at indicated time points. **E,** After 72 hours of treatment, cells from each condition were labeled with BrdU over 2 hours and quantified by flow cytometry (representative of three independent replicates). **F,** Annexin V and propidium iodide staining was analyzed by flow cytometry ($n = 3$ independent replicates). **G,** At 96 hours after treatment, 1×10^5 cells were plated in soft agar, in triplicate, for each condition. Colonies were counted at 4 weeks (FT246) or 10 weeks (FT194) after seeding. Scale bar, 50 μm. Statistical comparisons analyzed by unpaired *t* test, two-tailed. Data are means ± SEM ($n = 3$). *, $P < 0.05$, **, $P < 0.01$.

Downloaded from cancerres.aacrjournals.org on December 8, 2019. © 2019 American Association for Cancer Research.

Published OnlineFirst September 17, 2019; DOI: 10.1158/0008-5472.CAN-18-3029

(Fig. 1D), as a result of the combined effects of reduced proliferation and increased apoptosis (Fig. 1E and F; Supplementary Fig. S1E).

Next, to assess transformation potential, cells treated for 96 hours with Mps1_i + CENP-E_i or vehicle were replated in soft agar. For FT194, which are unable to form colonies in soft agar, small colonies emerged at around 10 weeks from cells that were pretreated with Mps1_i + CENP-E_i (Fig. 1G). Although FT246 cells form small colonies even under normal growth conditions, by 3 weeks after treatment with Mps1_i + CENP-E_i, the colonies were more numerous and larger compared with controls. We conclude that although CIN impairs cell viability and growth acutely, it enables the evolution of transformed colonies by generating genetic diversity.

CIN/aneuploidy causes proteotoxic stress and confers selective vulnerability to proteasome inhibition in fallopian tube secretory cells

We hypothesized that the detrimental effects of CIN/aneuploidy in FTSECs may be, at least in part, due to proteotoxic stress. Excess proteins produced by additional chromosomes result in protein stoichiometry imbalances, placing increased burden on protein degradation machinery to prevent accumulation of misfolded protein, which compromise cellular function and viability (6, 7, 10). Consistent with this model, detergent-insoluble ubiquinated proteins accumulated following chromosome missegregation (Fig. 2A), and Thioflavin T, a fluorescent dye that binds to amyloid fibrils, highlighted numerous intracellular aggregates of misfolded protein (Fig. 2B).

Western blotting of cell lysates revealed increased levels of the ER chaperone, BiP in FT246 cells, but not in FT194 cells (Fig. 2C). Increased phosphorylation of the translation initiation factor eIF2α, which attenuates general mRNA translation (11, 26), and induction of its downstream targets, the transcription factor ATF4 and the proapoptotic protein CHOP, were observed beginning after 48-hour exposure to Mps1_i + CENP-E_i, particularly in FT194 cells. No differences in ATF6 cleavage or XBP-1 splicing were observed (Fig. 2C; Supplementary Fig. S1F). Collectively, these findings indicate that the UPR is activated through an eIF2α-mediated stress pathway in FTSECs with CIN. We noted cell line–specific engagement of UPR effector pathways, specifically p-eIF2α induction was pronounced in FT194 cells, whereas marked upregulation of BiP was observed in FT246 cells.

Previous work has demonstrated the induction of an autophagic response and its inability to effectively digest misfolded protein aggregates that accumulate following chromosome missegregation (10). During autophagy, the cytosolic form of LC3, referred to as LC3-I, is conjugated to phosphatidylethanolamine to form lipidated LC3, otherwise known as LC3-II, which is recruited to autophagosomal membranes (27). In our model system of CIN/aneuploidy, we observed increased generation of LC3-II, which was further enhanced upon inhibition of autophagosome-lysosome fusion by the addition of Bafilomycin A1, demonstrating the dependency of these cells on autophagic flux (Supplementary Fig. S1G).

Quantification of nascent protein synthesis by incorporation of the methionine analogue homopropargylglycine (HPG) revealed progressive downregulation of protein synthesis over time (Fig. 2D), representing a compensatory mechanism to cope with the increased burden of misfolded protein. To determine the consequences of further proteostasis disruption, cells were treated with proteasome inhibitors, bortezomib or carfilzomib. FTSECs pretreated with Mps1_i + CENP-E_i showed a greater proportional decrease in viability after 48-hour proteasome inhibitor treatment compared with DMSO-pretreated cells, indicating that CIN/aneuploidy confers vulnerability to exacerbation of proteotoxic stress (Fig. 2E).

Increasing CIN is cytotoxic to ovarian cancer cells

We next investigated the consequences of increasing CIN in ovarian cancer cells, including two HGSOC cell lines (TOV1946 and TOV2223), and three cell lines likely derived from nonserous ovarian tumors (SKOV3, TOV21G, and A2780; refs. 28, 29). FACS analysis confirmed ploidy heterogeneity after 48 hours of dual Mps1/CENP-E inhibition (Fig. 3A). Compared with untransformed FTSECs, cancer cells were generally less tolerant to further increases in CIN, particularly for TOV21G and A2780 cell lines, which harbor inactivating mutations in *PTEN*, but no mutations in *TP53* (Fig. 3B). Mps1_i + CENP-E_i pretreatment caused modest sensitization to bortezomib in TOV1946 and TOV2223 cells but not in TOV21G cells, likely due to eradication of the cellular fraction susceptible to proteotoxic stress upfront by chromosome missegregation (Fig. 3C).

Ovarian cancer spheroids downregulate mTORC1, attenuate translation, and acquire resistance to bortezomib

The selective vulnerability of aneuploid cells to proteasome inhibition suggests that HGSOC, one of the most highly aneuploid malignancies, should be responsive to proteasome inhibitors. However, clinical trials have demonstrated poor response rates to bortezomib in ovarian cancer patients (30, 31). Consistent with previous work (32), we observed that inhibition of translation by cycloheximide was protective against bortezomib-induced cytotoxicity, indicating that decreased protein synthesis alleviates the sensitivity of cells to proteasomal inhibition (Fig. 3D). We therefore speculated that modulation of protein synthesis rate could be an important contributing factor.

A unique characteristic of ovarian carcinoma is its propensity to grow as detached spheroids suspended in the ascites fluid within the peritoneal cavity. Strikingly, we observed increased resistance to proteasome inhibitors in cell lines grown as spheroids compared with adherent monolayer cultures, using two different cell viability assays quantifying cellular ATP or total DNA content (Fig. 4A; Supplementary Fig. S2A and S2B). To gain further insight into the resistance mechanism in tumor spheroids, we transduced TOV1946 cells with a proteasome activity reporter comprised of a green fluorescent protein (ZsGreen) fused to mouse ornithine decarboxylase (mODC) and independently expressing mCherry through an IRES linkage (17). Ornithine decarboxylase is normally rapidly degraded in cells with active proteasomal machinery. In cells with low proteasome activity, the ZsGreen–mODC fusion protein accumulates, leading to emission of green fluorescence. Under standard media conditions, we observed that cells grown either in adherent monolayer or in spheroid cultures expressed minimal green fluorescence, indicating proteasome activity under both conditions. However, 24 hours after the addition of bortezomib, all cells grown under adherent conditions were uniformly fluorescent, whereas in spheroids,

Downloaded from cancerres.aacrjournals.org on December 8, 2019. © 2019 American Association for Cancer Research.

Published OnlineFirst September 17, 2019; DOI: 10.1158/0008-5472.CAN-18-3029

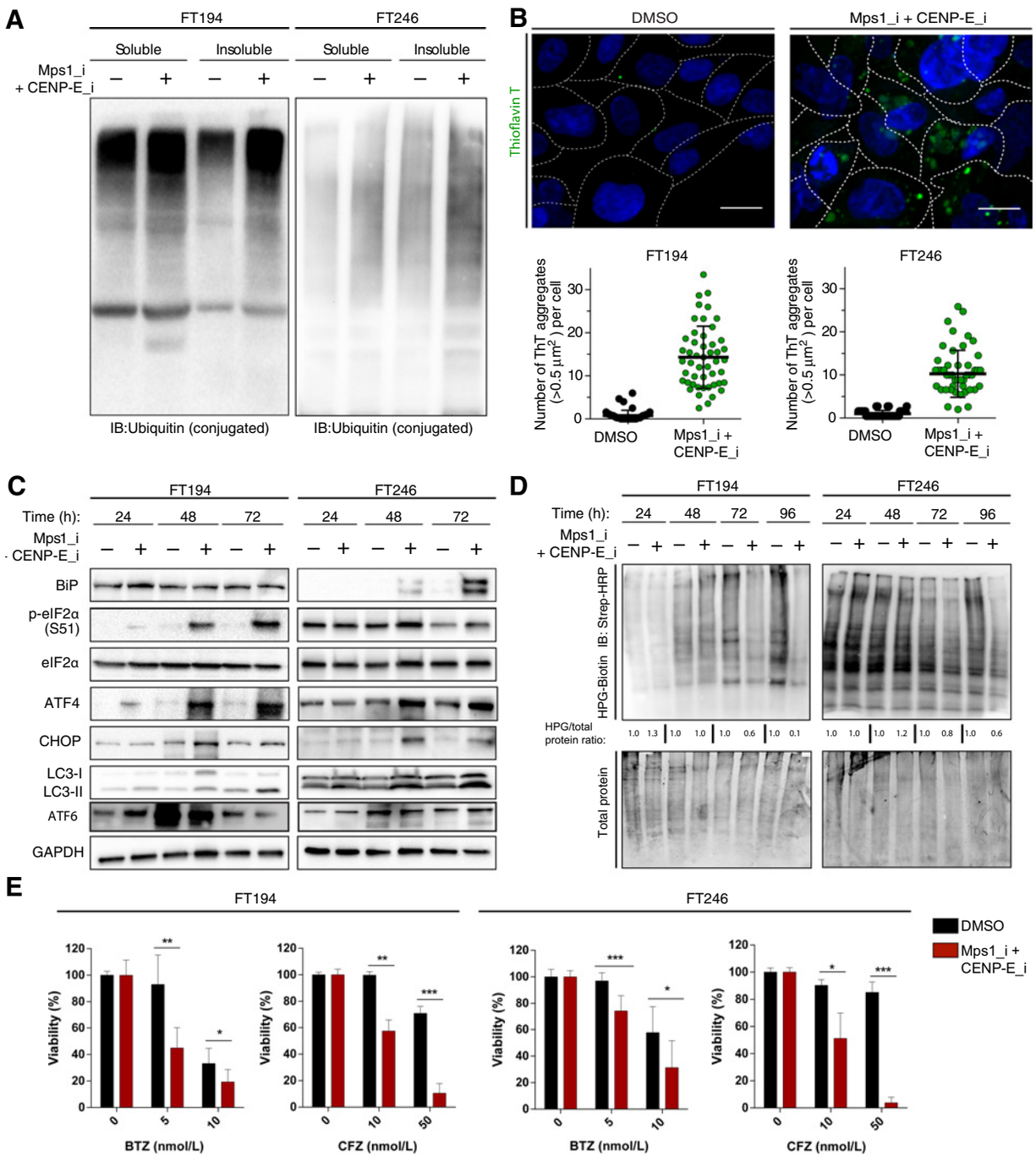

Figure 2.

Chromosome missegregation in FTSECs leads to accumulation of aggregated protein, ER stress, and sensitivity to bortezomib. Cells were treated with Mps1_i + CENPE_i or DMSO and analyzed 72 hours later. **A,** Equal numbers of cells from each condition were collected and lysed in Triton-X. Lysates were separated into detergent-soluble and insoluble fractions and immunoblotted for ubiquitinated proteins. **B,** Fixed cells (FT194) were stained with Thioflavin T for visualization of protein aggregates. At least 500 cells were quantified per condition. Scale bar, 10 µm. **C,** Total cell lysates were harvested at the indicated time points following treatment and subjected to immunoblotting for UPR and autophagy markers. **D,** Newly synthesized protein over 2-hour metabolic labeling, normalized to total protein levels (Coomassie). For each time point, the ratio of HPG-labeled/total protein was determined by densitometry in Mps1_i + CENP-E_i-treated cells relative to control. **E,** Cells were treated with bortezomib (BTZ) or carfilzomib (CFZ) at indicated concentrations (or vehicle control) for 48 hours. Cell viability was assessed by ATP luminescence assay. Statistical comparisons were computed by an unpaired *t* test, two-tailed, with Welch correction. Data are means ± SEM ($n = 3$). *, $P < 0.05$; **, $P < 0.01$; ***, $P < 0.001$.

Downloaded from cancerres.aacrjournals.org on December 8, 2019. © 2019 American Association for Cancer Research.

Published OnlineFirst September 17, 2019; DOI: 10.1158/0008-5472.CAN-18-3029

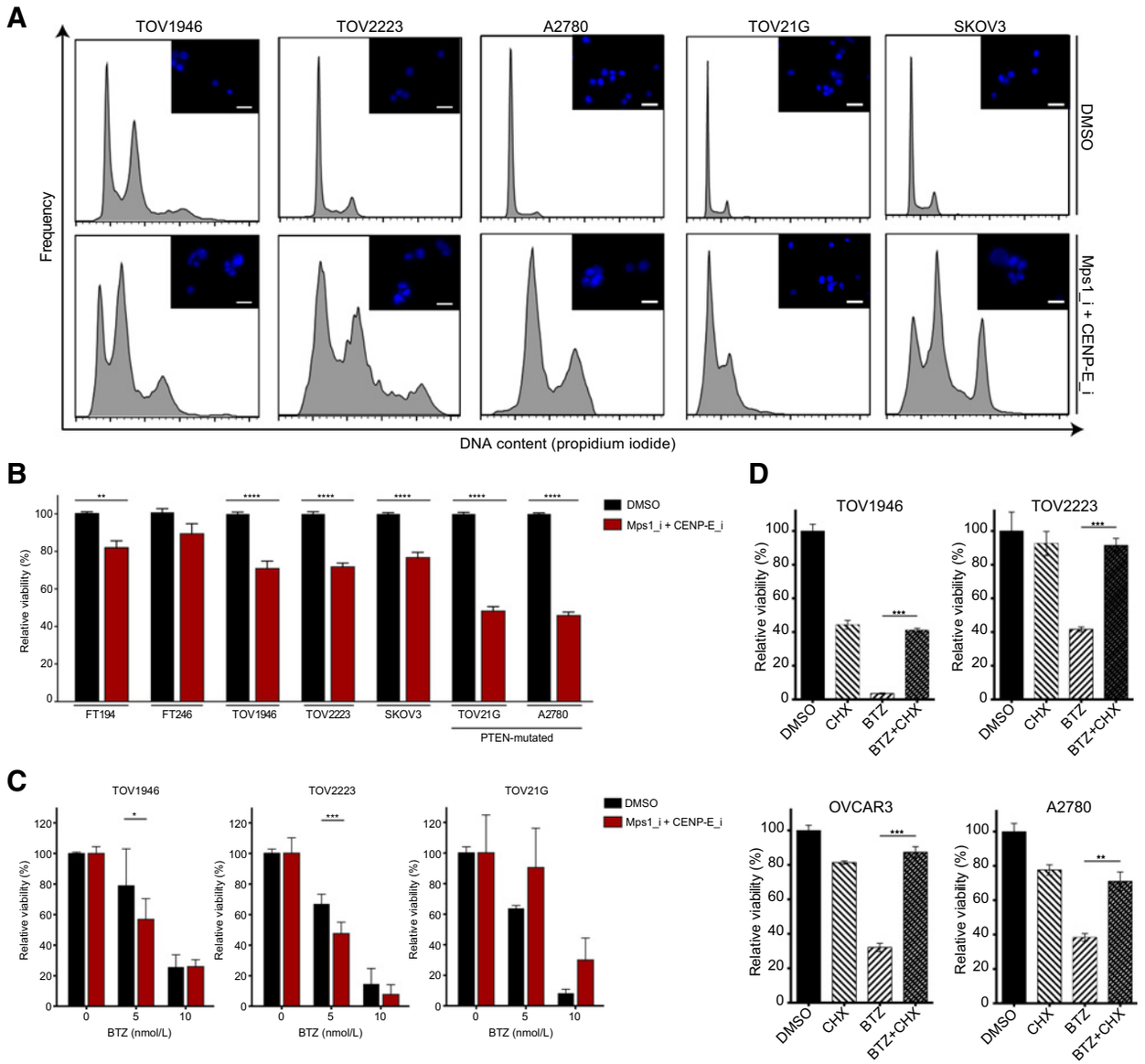

Figure 3.

Pharmacologically induced chromosome missegregation and proteasome inhibition is cytotoxic to ovarian cancer cells, whereas cycloheximide protects against proteotoxicity. **A,** Cell lines were treated with Mps1_i + CENP-E_i or DMSO for 48 hours and DNA content, by propidium iodide staining, was assessed by flow cytometry. **B,** Cell viability was assessed by ATP luminescence assay. **C,** After 48-hour exposure to Mps1_i + CENP-E_i or DMSO, cells were treated with bortezomib at indicated concentrations (or vehicle control) for 48 hours. Cell viability was assessed by ATP luminescence assay. **D,** Relative cell viability 48 hours after treatment with vehicle, 10 nmol/L bortezomib (BTZ), or bortezomib with 0.5 μg/mL cycloheximide (CHX), quantified by ATP luminescence assay. Statistical comparisons computed by unpaired *t* test, two-tailed. Data are means ± SEM ($n = 3$). *, $P < 0.05$; **, $P < 0.01$; ***, $P < 0.001$; ****, $P < 0.0001$.

fluorescence was localized to cells at the periphery (Fig. 4B; Supplementary Fig. S2C). This observation suggested that translation rates might be reduced in cells positioned within the inner core of spheroids, preventing the accumulation of the reporter protein despite proteasome inhibition. Alternatively, bortezomib may not be able to penetrate efficiently into the spheroid core. Lastly, proteasomal activity could be modulated in spheroids such that activity remains high in the spheroid core and decreased at the periphery. We therefore measured global protein synthesis in adherent and spheroid cultures and demonstrated decreased synthetic rates in spheroids compared with adherent cultures (Fig. 4C). Exposure of HGSOC spheroids to HPG conjugated to a fluorescent dye revealed decreased protein synthesis (Fig. 4D).

We speculated that attenuation of mTORC1 activity, a critical regulatory control point for protein synthesis, may mediate reduced translational in the spheroid core. We noted reduced levels of two established mTORC1 substrates, p-4E-BP1 and p-S6 ribosomal protein, in established PTEN-sufficient ovarian cancer cell lines and in freshly derived tumor spheroids cultured from

Downloaded from cancerres.aacrjournals.org on December 8, 2019. © 2019 American Association for Cancer Research.

Published OnlineFirst September 17, 2019; DOI: 10.1158/0008-5472.CAN-18-3029

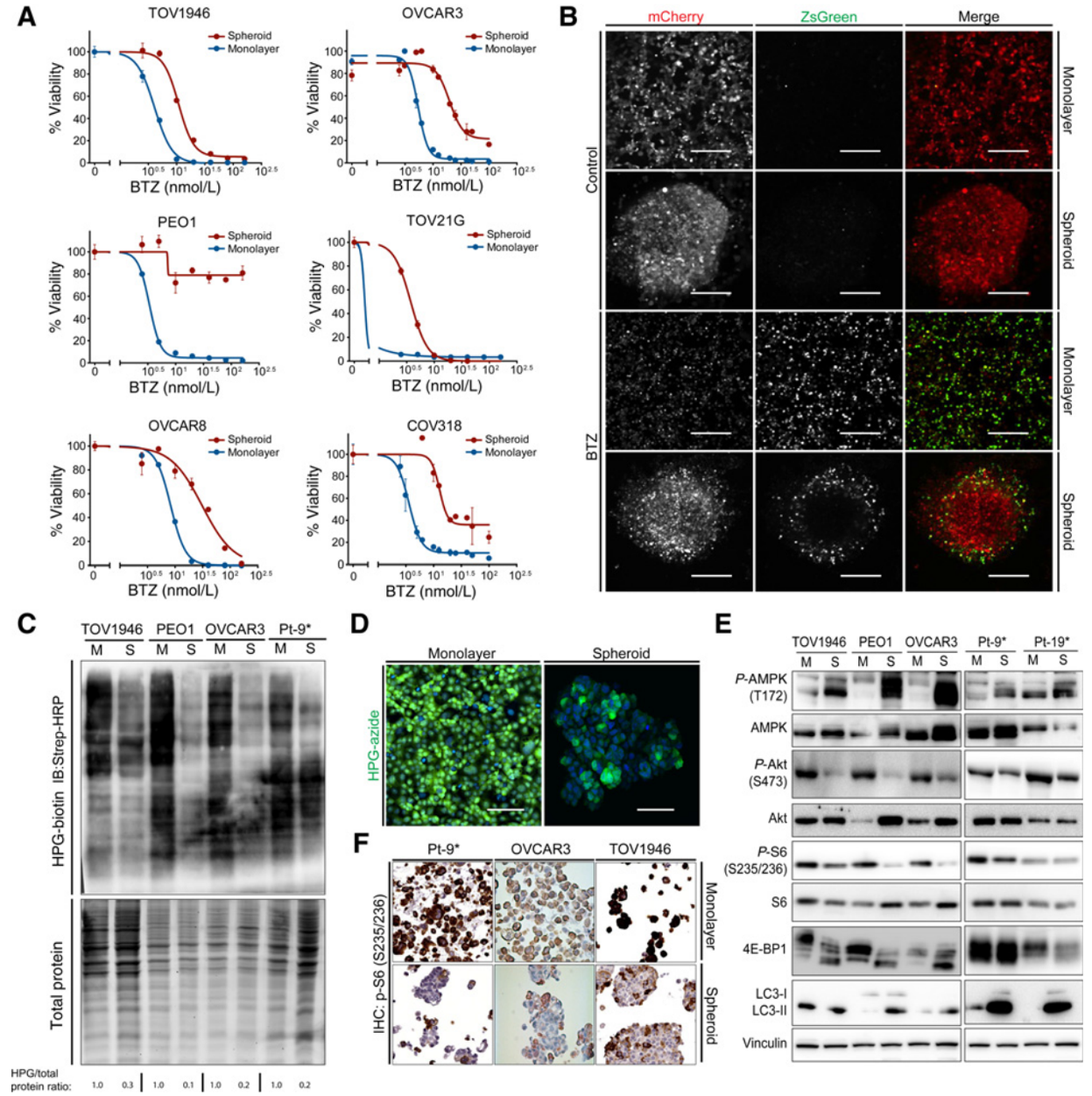

Figure 4.

Resistance to bortezomib in ovarian cancer spheroids is associated with downregulation of mTORC1 and protein synthesis inhibition. **A,** Ovarian cancer cell lines were grown in either adherent monolayer or spheroid cultures in parallel and treated with bortezomib at increasing concentrations. Cell viability was determined at 48 hours by ATP luminescence assay. **B,** TOV1946 cells stably expressing pLVX-ZsGreen-mODC-IRES-mCherry were grown either in monolayer or spheroids, in the presence of bortezomib (5 nmol/L) or vehicle control for 48 hours, and visualized by confocal microscopy. Scale bar, 200 μm. **C,** Newly synthesized protein over 2-hour labeling period performed concurrently in adherent monolayer and spheroid cultures, normalized over total protein (Coomassie). **D,** TOV1946 cells, monolayer and spheroid cultures, labeled by HPG over 2 hours, followed by conjugation to a green fluorescent dye. Scale bar, 50 μm. **E,** Western blotting of cell lysates from HGSOC cell lines (TOV1946, OVCAR3, and PEO1) and short-term cultures of primary patient-derived HGSOC cells from ascites (Pt-9 and Pt-19, both with retained PTEN expression and *PIK3CA* wild-type) grown as spheroids or adherent monolayer cultures. **F,** Immunohistochemical (IHC) staining for p-S6 (S235/236) performed on spheroids and cell pellets from monolayer culture.

HGSOC ascites suggestive of reduced mTORC1 catalytic activity (Fig. 4E; Supplementary Fig. S3A). We examined how the growth conditions of HGSOC cells modulated the activity of AMPK, a major negative regulator of mTORC1. We observed high levels of p-AMPK, indicative of bioenergetic stress, and increased autophagic activity as measured by levels of LC3-II in tumor spheroids compared with cells grown in monolayer. Consistent with these findings, we observed diffuse p-S6 immunostaining in

Downloaded from cancerres.aacrjournals.org on December 8, 2019. © 2019 American Association for Cancer Research.

Published OnlineFirst September 17, 2019; DOI: 10.1158/0008-5472.CAN-18-3029

cells grown under adherent monolayer conditions, whereas decreased staining was observed in spheroids (Fig. 4F). Pax-8 immunostaining confirmed Müllerian epithelial differentiation (Supplementary Fig. S3B). Modulation of translation rate may thus be an adaptive mechanism to the bioenergetic stress intrinsic to spheroid growth protecting these cells from the cytotoxic effects of proteasome inhibition.

PTEN loss is associated with UPR activation in high-grade serous carcinoma

Loss of PTEN expression, as determined by negative immunohistochemical staining of tumor cells, has been observed at frequencies ranging from 12% to 25% in cohorts of HGSOC (33); 6% are attributed to homozygous deletion, <1% due to mutations, and the remaining due to other genetic or epigenetic mechanisms (2, 33). The rate of hemizygous deletion occurs in 36% of all HGSOCs, suggesting that haploinsufficiency may be selected for in this tumor (2).

Because PTEN deficiency enforces high mTORC1 activation, we conjectured that tumors lacking PTEN might exhibit elevated translation rates, resulting in a higher burden of proteotoxic stress. Gene set enrichment analysis of the TCGA HGSOC gene-expression data set (2) revealed a positive correlation of expressed genes involved in mTORC1 and UPR signaling (Fig. 5A and B). To validate this relationship in an independent cohort, immunohistochemical staining for PTEN and p-eIF2α was performed on a tissue microarray of 128 primary ovarian carcinomas, revealing significantly increased p-eIF2α staining in tumors with complete PTEN loss ($n = 21$), compared with tumors that retained PTEN expression ($n = 107$; $P < 0.0001$, Mann–Whitney test; Fig. 5C). Knockdown of PTEN in ovarian cancer cells caused an increase in protein synthesis, measured by HPG incorporation assay (Fig. 5D), and was associated with upregulation of BiP and increased levels of p-eIF2α and CHOP (Fig. 5E). Overall, the data are consistent with cross-talk between the PTEN/PI3K/mTORC1 and UPR activation in HGSOC.

mTORC1 activation potentiates aneuploidy-associated UPR induction

Loss of PTEN is an early pathogenic event in HGSOC, occurring in fallopian tube precursor lesions (12, 34). We therefore sought to study the combined effects of PTEN loss and aneuploidy in fallopian tube epithelium. Knockdown of PTEN resulted in increased protein synthesis in FT194 cells (Supplementary Fig. S4A). We observed significantly higher basal levels of p-eIF2α upon depletion of PTEN, with modest further elevations following Mps1_i + CENP-E_i treatment (Fig. 5F). Confirming that the effects are due to mTORC1 activation, similar results were obtained comparing $TSC2^{-/-}$ MEFs with $TSC2^{+/+}$ MEFs in response to Mps1_i + CENP-E_i. We also observed that, unlike wild-type MEFs, which eventually recovered from the proliferative arrest when replated in drug-free media, $TSC^{-/-}$ MEFs were unable to do so (Supplementary Fig. S4B and S4C).

Loss of PTEN sensitizes to bortezomib in models of HGSOC

Clinical development of mTOR inhibitors to treat cancers driven by high levels of PI3K/mTORC1 activation has proven largely ineffective (35, 36). We observed that although nanomolar concentrations of rapamycin potently suppressed mTORC1 signaling, it failed to elicit cell death and exerted only modest cytostatic effects, even in PTEN-deficient cells (Supplementary Fig. S4D–S4H). Moreover, rapamycin mitigated proteotoxic stress, as evidenced by the lack of BiP induction following PTEN depletion (Supplementary Fig. S4I). We next tested the effect of proteasome inhibition on TOV1946 cells with PTEN depleted by RNA interference. PTEN-deficient cells were significantly more sensitive to bortezomib compared with shGFP-transduced controls, under both monolayer and spheroid culture conditions (Fig. 6A; Supplementary Fig. S5A and S5B). Compared with $TOV1946^{shGFP}$ cells, $TOV1946^{shPTEN}$ cells demonstrated higher basal levels of BiP, p-eiF2α, ATF4, and CHOP (Fig. 6B). In response to bortezomib, loss of PTEN was associated with further elevations of BiP and p-eiF2α, along with early and transient induction of ATF4. Increased levels of the downstream effector CHOP became evident at 12 hours after treatment, which were more pronounced in shPTEN-transduced cells relative to control. The effects of proteasome inhibition on ATF6 and LC3-II levels do not appear to be affected by PTEN status. Hyperactivation of UPR signaling in $TOV1946^{shPTEN}$ was associated with increased accumulation of ubiquitinated proteins and formation of protein aggregates (Fig. 6C). Similar results were observed with knockdown of TSC2, the most proximal suppressor of mTORC1 (Supplementary Fig. S5C–S5E).

We next tested whether PTEN loss sensitized to bortezomib in a xenograft model that recapitulates the peritoneal dissemination observed in HGSOC (Supplementary Fig. S6A and S6B). Luciferase-expressing TOV1946 cells were infected with hairpins against PTEN or GFP and injected into the peritoneal cavity of NOD/SCID/IL2Rγ$^{-/-}$ mice. Mice were treated with bortezomib, 1.0 mg/kg or PBS twice weekly, as previously described (37), starting at 2 weeks after inoculation of tumor cells. Bioluminescence imaging revealed a marked reduction in tumor growth in $TOV1946^{shPTEN}$ xenografts treated with drug compared with controls (Fig. 6D and E). These results demonstrate enhanced efficacy of proteasome inhibition in HGSOC cells lacking PTEN expression in both *in vitro* spheroid conditions and *in vivo* models.

Discussion

Histopathologic studies have identified the FTSEC as the cell of origin of the majority of HGSOCs (1, 12). It is thought that mutation in *TP53* is an early event in the pathogenesis of HGSOC, as abnormal nuclear localization of p53 protein is observed in the precursor lesion, serous tubal intraepithelial carcinoma, and in adjacent morphologically normal FTSECs (38). The latter finding suggests that the acquisition of genomic instability occurs after mutation in *TP53*. This is consistent with the study by Ohashi and colleagues showing that aneuploidy causes p53-mediated apoptosis (4). Thus, loss of p53 tumor suppressor function may be a prerequisite for cells to tolerate CIN. Notably, we observed that *TP53*-wild-type ovarian cancer cell lines A2780 and TOV21G cells, likely derived from endometrioid and clear cell carcinoma, respectively (28, 29), were particularly sensitive to chromosome missegregation.

We sought to model the process of aneuploidy acquisition *in vitro*, using the immortalized, but nontumorigenic cell lines, FT194 and FT246, derived from primary FTSECs by enforced expression of SV40 large T-antigen or hTERT/$CDK4^{R24C}$/shTP53, respectively (21). Our finding that cell viability and proliferation are compromised after inducing chromosome missegregation (in

Downloaded from cancerres.aacrjournals.org on December 8, 2019. © 2019 American Association for Cancer Research.

Published OnlineFirst September 17, 2019; DOI: 10.1158/0008-5472.CAN-18-3029

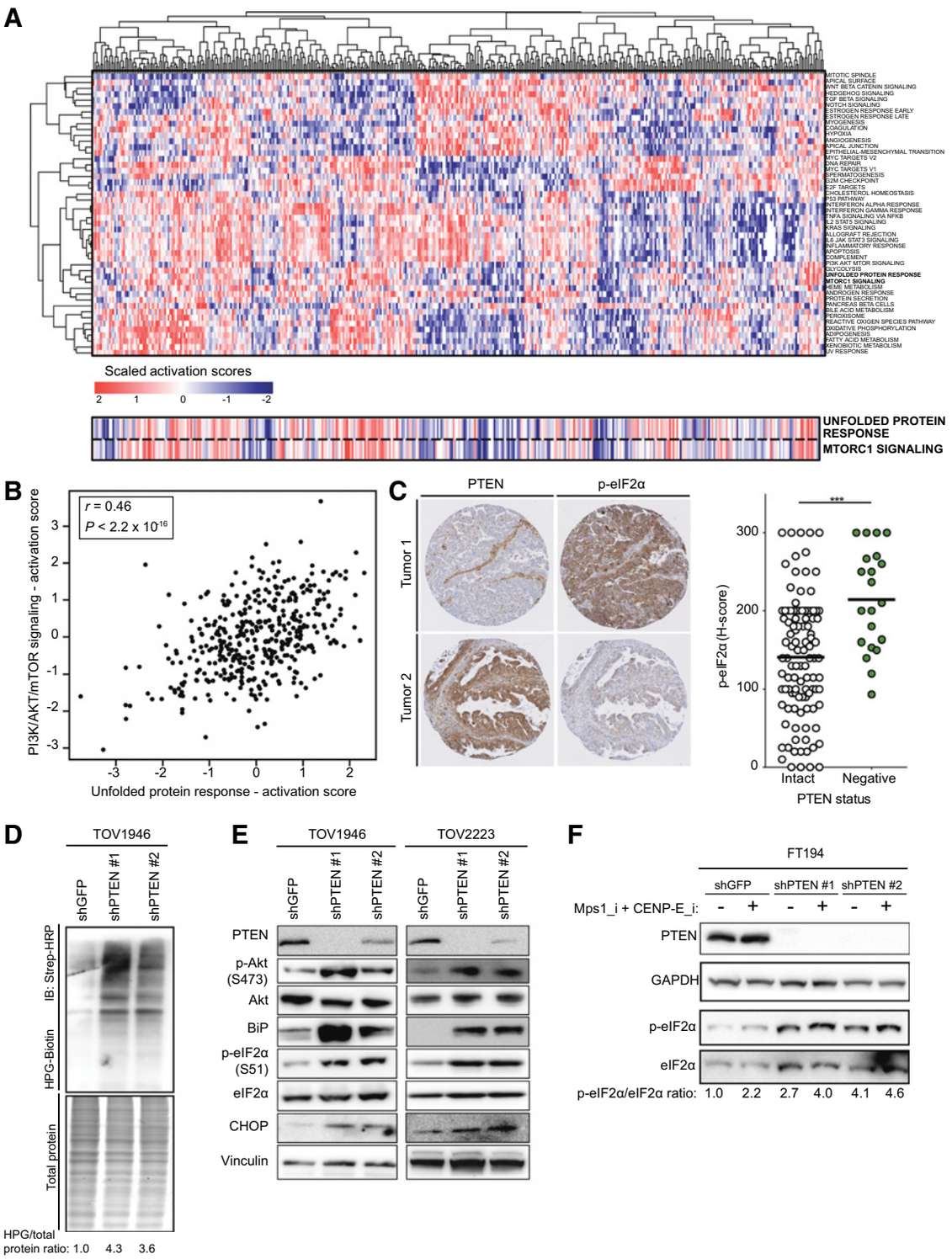

Figure 5.

mTORC1 and UPR cross-talk in HGSOC. **A,** Gene set enrichment analysis of mRNA expression of HGSOC from TCGA data set. **B,** Correlation between mTORC1 and UPR signature activation scores. **C,** Immunohistochemical staining for PTEN and p-eIF2α in a cohort of 128 ovarian carcinomas. Statistical comparisons were computed by Mann–Whitney *U* test, two-sided. ***, $P < 0.0001$. **D,** HPG incorporation over 2 hours in TOV1946 cells transduced with shRNAs against PTEN or GFP (control). **E,** Immunoblot of PTEN-knockdown versus control cells. **F,** FT194 cells transduced with shRNAs against PTEN or GFP were treated with Mps1_i + CENP-E_i for 48 hours and subjected to immunoblot.

Downloaded from cancerres.aacrjournals.org on December 8, 2019. © 2019 American Association for Cancer Research.

Published OnlineFirst September 17, 2019; DOI: 10.1158/0008-5472.CAN-18-3029

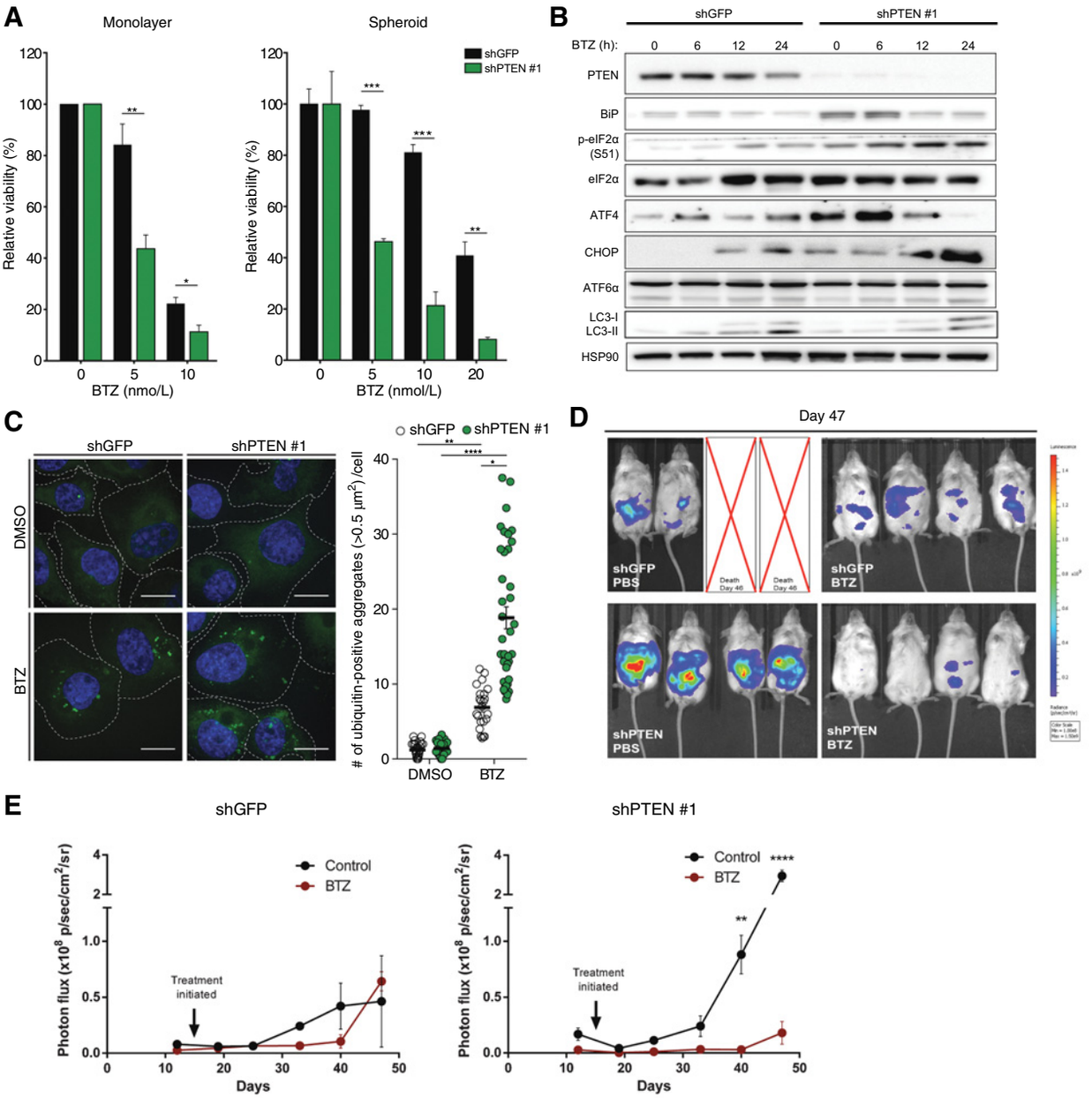

Figure 6.

PTEN loss sensitizes to bortezomib. **A,** Cell viability was assessed 48 hours after bortezomib treatment of TOV1946shGFP and TOV1946shPTEN cells grown in monolayer adherent and spheroid cultures. Statistical comparisons were computed by two-way ANOVA with Bonferroni correction. **B,** TOV1946 cells were treated with bortezomib, and cell lysates were analyzed by Western blotting at the indicated time points. **C,** Immunofluorescence for ubiquitinylated proteins 24 hours after treatment; at least 100 cells analyzed per condition. Scale bar, 20 μm. **D** and **E,** NSG mice received intraperitoneal injections of TOV1946^{Luc} cells stably expressing shGFP or shPTEN#1 and were treated with bortezomib 1.0 mg/kg or PBS twice weekly ($n = 5$ per group). **D,** Bioluminescence imaging of mice alive on day 47 after tumor inoculation. **E,** Bioluminescence readings were monitored weekly after tumor inoculation. Statistical comparisons were computed by unpaired *t* tests, two-tailed, at 40- and 47-day time points. *, $P < 0.05$; **, $P < 0.01$; ***, $P < 0.001$; ****, $P < 0.0001$.

the context of p53 loss of function) indicates that p53-independent mechanisms are operating to resist survival of aneuploid cells.

Strikingly, despite short-term impairment of cellular fitness, chromosome missegregation generates genomic diversity, enabling the emergence of transformed clones. Random aneuploidy has been shown to give rise to clones with a fitness advantage under stressful conditions (39). However, as we observed, transformed cells appear to be less tolerant of further increasing CIN, implicating the importance of genetic background and basal rate of genomic instability in determining the outcome of mitotic checkpoint inhibition.

Downloaded from cancerres.aacrjournals.org on December 8, 2019. © 2019 American Association for Cancer Research.

Published OnlineFirst September 17, 2019; DOI: 10.1158/0008-5472.CAN-18-3029

Several groups have demonstrated that aneuploidy causes proteotoxic stress in cell culture models (4–6, 9, 10). We demonstrate here that ER stress and UPR activation can be induced in response to CIN in immortalized human FTSECs, and therefore, may potentially be involved in the early pathogenesis of HGSOC. To cope with these changes, cells adapt by decreasing translation and increasing protein degradation.

HGSOC cells are in a state of elevated proteotoxic stress due to CIN and elevated protein synthesis rates resulting from activation of anabolic pathways, including PI3K/AKT and Myc (2), which may be compounded with their native function as secretory cells. Accordingly, inhibition of protein degradation, which represents a major mechanism by which cells adapt to and alleviate proteotoxic stress, provokes irreversible cytotoxicity in aneuploid FTSECs and HGSOC cells. As these observations are at odds with the poor efficacy of bortezomib in clinical trials of ovarian cancer patients (30, 31), we sought to uncover potential mechanisms of therapeutic resistance. We show that ovarian cancer cells acquire resistance to bortezomib when grown as three-dimensional spheroids, wherein they adopt a metabolically quiescent state, characterized by AMPK activation, reduced mTORC1 signaling and translational attenuation, which serve to protect these cells from proteotoxic stress. Hence, the data posit that tumor spheroids propagating in the ascites of patients with advanced disease may be resistant to bortezomib.

Enforced high mTORC1 activity by depletion of PTEN restored sensitivity to bortezomib in tumor spheroids. In TOV1946^{shPTEN} xenografts, cancer cells adapted to PTEN silencing over the course of several weeks, forming malignant ascites. Treatment with bortezomib significantly decreased tumor burden. Future studies should evaluate the efficacy of proteasome inhibition in genetically engineered mouse models and patient-derived xenograft models of PTEN-deficient ovarian tumors.

Other genetic alterations that enhance mTORC1 activity (gene amplification or activating mutations of PIK3CA, AKT, or RHEB, or loss of suppressors, TSC1 or TSC2) are predicted to cause similar effects. Data from the Genomics of Drug Sensitivity in Cancer Project, which comprise small-molecule compound screens performed on a panel of 426 cancer cell lines, show a significant positive association between *PTEN* mutation and increased sensitivity to the proteasome inhibitor, MG-132 ($P = 0.040$), and even more robust associations between *PIK3CA* mutation and increased sensitivity to bortezomib ($P = 0.0035$) and MG-132 ($P = 0.008$), which further support this hypothesis (40).

PTEN is the member of the PI3K/mTORC1 pathway most frequently altered in ovarian cancer, which occurs at a higher frequency in endometrioid and clear cell ovarian cancers. Because these tumors typically have fewer gene copy-number alterations and are driven primarily by point mutations (1), the extent of aneuploidy that is sufficient to confer cells with vulnerability to proteasome inhibition is a relevant question that deserves further investigation. Endometrioid and clear cell tumors can also show significant secretory activity by histomorphology (41, 42), suggesting that they may be prone to agents that exacerbate ER stress.

Development of therapies to treat tumors with constitutive PI3K/AKT/mTOR signaling has focused on inhibiting the kinase components of this pathway. Clinical trials of mTOR inhibitors in ovarian cancer patients have been disappointing, and treatment response did not correlate with markers of mTOR activity (35, 36). Rapamacyin is well known to exert cytostatic, rather than cytotoxic effects and, in some contexts, stimulates Akt to promote survival (43). Our data show that inhibition of mTORC1 reduces translation and quells elevated proteotoxic stress, leading to bortezomib resistance.

We have demonstrated in a model of FTSEC transformation that aneuploidy compromises cellular fitness by causing ER stress. CIN/aneuploidy engenders an emergent vulnerability to protein homeostasis disruption, such that proteasome inhibition triggers a proteotoxic cell death program. Dormant HGSOC cells within tumor spheroids are able to buffer the cytotoxic effects of bortezomib by suppressing protein synthesis by AMPK-mediated downregulation of mTORC1. *In vitro* culture spheroids may thus recapitulate one aspect of the cellular state of ovarian cancer cells in malignant ascites. In contrast, constitutive activation of mTORC1 in PTEN-deficient tumors increases ER stress, even in spheroids. Markers of mTORC1 activation, such as PTEN loss, may therefore potentially identify cancer patients who may be responsive to proteasome inhibitors or other emerging therapeutic agents targeting proteostasis.

Disclosure of Potential Conflicts of Interest

R.E. Tiedemann is a consultant for Janssen and Amgen. R. Drapkin is a scientific advisory board member for Repare Therapeutics and Siamab Therapeutics. R. Rottapel is a founding member of Northern Biologics. No potential conflicts of interest were disclosed by the other authors.

Authors' Contributions

Conception and design: M.H. Chui, R. Rottapel
Development of methodology: M.H. Chui
Acquisition of data (provided animals, acquired and managed patients, provided facilities, etc.): M.H. Chui, S.A. Doodnauth, N. Erdmann, R.E. Tiedemann, R. Drapkin, P. Shaw
Analysis and interpretation of data (e.g., statistical analysis, biostatistics, computational analysis): M.H. Chui, S.A. Doodnauth, N. Erdmann, F. Sircoulomb
Writing, review, and/or revision of the manuscript: M.H. Chui, F. Sircoulomb, R. Drapkin, P. Shaw, R. Rottapel
Administrative, technical, or material support (i.e., reporting or organizing data, constructing databases): S.A. Doodnauth, R.E. Tiedemann, P. Shaw
Study supervision: R. Rottapel

Acknowledgments

M.H. Chui was supported by a CIHR Post-Doctoral Fellowship Award. This work was supported by grants to R. Rottapel from Canadian Institute for Health Research (CIHR FDN 143230), and the Ontario Institute for Cancer Research (OC TRI FR22B). The authors wish to thank Dr. Vuk Stambolic for helpful discussions and provision of TSC$^{-/-}$ cells.

The costs of publication of this article were defrayed in part by the payment of page charges. This article must therefore be hereby marked *advertisement* in accordance with 18 U.S.C. Section 1734 solely to indicate this fact.

Received October 16, 2018; revised July 25, 2019; accepted September 9, 2019; published first September 17, 2019.

References

1. Kurman RJ, Shih IM. The dualistic model of ovarian carcinogenesis: revisited, revised, and expanded. Am J Pathol 2016;186:733–47.
2. The Cancer Genome Atlas Research Network. Integrated genomic analyses of ovarian carcinoma. Nature 2011;474:609–15.

Downloaded from cancerres.aacrjournals.org on December 8, 2019. © 2019 American Association for Cancer Research.

Published OnlineFirst September 17, 2019; DOI: 10.1158/0008-5472.CAN-18-3029

3. Cope L, Wu RC, Shih Ie M, Wang TL. High level of chromosomal aberration in ovarian cancer genome correlates with poor clinical outcome. Gynecol Oncol 2013;128:500–5.
4. Ohashi A, Ohori M, Iwai K, Nakayama Y, Nambu T, Morishita D, et al. Aneuploidy generates proteotoxic stress and DNA damage concurrently with p53-mediated post-mitotic apoptosis in SAC-impaired cells. Nat Commun 2015;6:7668.
5. Williams BR, Prabhu VR, Hunter KE, Glazier CM, Whittaker CA, Housman DE, et al. Aneuploidy affects proliferation and spontaneous immortalization in mammalian cells. Science 2008;322:703–9.
6. Oromendia AB, Dodgson SE, Amon A. Aneuploidy causes proteotoxic stress in yeast. Genes Dev 2012;26:2696–708.
7. Santaguida S, Amon A. Short- and long-term effects of chromosome mis-segregation and aneuploidy. Nat Rev Mol Cell Biol 2015;16:473–85.
8. Sheltzer JM, Ko JH, Replogle JM, Habibe Burgos NC, Chung ES, Meehl CM, et al. Single-chromosome gains commonly function as tumor suppressors. Cancer Cell 2017;31:240–55.
9. Stingele S, Stoehr G, Peplowska K, Cox J, Mann M, Storchova Z. Global analysis of genome, transcriptome and proteome reveals the response to aneuploidy in human cells. Mol Syst Biol 2012;8:40.
10. Santaguida S, Vasile E, White E, Amon A. Aneuploidy-induced cellular stresses limit autophagic degradation. Genes Dev 2015;29:2010–21.
11. Ron D, Walter P. Signal integration in the endoplasmic reticulum unfolded protein response. Nat Rev Mol Cell Biol 2007;8:519–29.
12. Labidi-Galy SI, Papp E, Hallberg D, Niknafs N, Adleff V, Noe M, et al. High grade serous ovarian carcinomas originate in the fallopian tube. Nat Commun 2017;8:1093.
13. Talamo TS, Bender BL, Ellis LD, Scioscia EA. Adenocarcinoma of the fallopian tube. An ultrastructural study. Virchows Arch A Pathol Anat Histol 1982;397:363–8.
14. Leung-Hagesteijn C, Erdmann N, Cheung G, Keats JJ, Stewart AK, Reece DE, et al. Xbp1s-negative tumor B cells and pre-plasmablasts mediate therapeutic proteasome inhibitor resistance in multiple myeloma. Cancer Cell 2013;24:289–304.
15. Aghajanian C, Dizon DS, Sabbatini P, Raizer JJ, Dupont J, Spriggs DR. Phase I trial of bortezomib and carboplatin in recurrent ovarian or primary peritoneal cancer. J Clin Oncol 2005;23:5943–9.
16. Levine DA, Bogomolniy F, Yee CJ, Lash A, Barakat RR, Borgen PI, et al. Frequent mutation of the PIK3CA gene in ovarian and breast cancers. Clin Cancer Res 2005;11:2875–8.
17. Stacer AC, Wang H, Fenner J, Dosch JS, Salomonnson A, Luker KE, et al. Imaging reporters for proteasome activity identify tumor- and metastasis-initiating cells. Mol Imaging 2015;14:414–32.
18. Medrano M, Communal L, Brown KR, Iwanicki M, Normand J, Paterson J, et al. Interrogation of functional cell-surface markers identifies CD151 dependency in high-grade serous ovarian cancer. Cell Rep 2017;18:2343–58.
19. Patch AM, Christie EL, Etemadmoghadam D, Garsed DW, George J, Fereday S, et al. Whole-genome characterization of chemoresistant ovarian cancer. Nature 2015;521:489–94.
20. Reich M, Liefeld T, Gould J, Lerner J, Tamayo P, Mesirov JP. GenePattern 2.0. Nat Genet 2006;38:500–1.
21. Karst AM, Levanon K, Drapkin R. Modeling high-grade serous ovarian carcinogenesis from the fallopian tube. PNAS 2011;108:7547–52.
22. Barisic M, Aguiar P, Geley S, Maiato H. Kinetochore motors drive congression of peripheral polar chromosomes by overcoming random arm-ejection forces. Nat Cell Biol 2014;16:1249–56.
23. Bennett A, Bechi B, Tighe A, Thompson S, Procter DJ, Taylor SS. Cenp-E inhibitor GSK923295: Novel synthetic route and use as a tool to generate aneuploidy. Oncotarget 2015;6:20921–32.
24. Santaguida S, Richardson A, Iyer DR, M'Saad O, Zasadil L, Knouse KA, et al. Chromosome mis-segregation generates cell-cycle-arrested cells with complex karyotypes that are eliminated by the immune system. Dev Cell 2017;41:638–51.e5.
25. Janssen A, van der Burg M, Szuhai K, Kops GJ, Medema RH. Chromosome segregation errors as a cause of DNA damage and structural chromosome aberrations. Science 2011;333:1895–8.
26. Harding HP, Zhang Y, Ron D. Protein translation and folding are coupled by an endoplasmic-reticulum-resident kinase. Nature 1999;397:271–4.
27. Tanida I, Ueno T, Kominami E. LC3 and autophagy. Methods in Mol Biol 2008;445:77–88.
28. Domcke S, Sinha R, Levine DA. Evaluating cell lines as tumour models by comparison of genomic profiles. Nat Commun 2013;4:2126.
29. Beaufort CM, Helmijr JC, Piskorz AM, Hoogstraat M, Ruigrok-Ritstier K, Besselink N, et al. Ovarian cancer cell line panel (OCCP): clinical importance of in vitro morphological subtypes. PLoS One 2014;9:e103988.
30. Ramirez PT, Landen CN Jr., Coleman RL, Milam MR, Levenback C, Johnston TA, et al. Phase I trial of the proteasome inhibitor bortezomib in combination with carboplatin in patients with platinum- and taxane-resistant ovarian cancer. Gynecol Oncol 2008;108:68–71.
31. Parma G, Mancari R, Del Conte G, Scambia G, Gadducci A, Hess D, et al. An open-label phase 2 study of twice-weekly bortezomib and intermittent pegylated liposomal doxorubicin in patients with ovarian cancer failing platinum-containing regimens. Int J Gynecol Cancer 2012;22:792–800.
32. Bazzaro M, Lin Z, Santillan A, Lee MK, Wang MC, Chan KC, et al. Ubiquitin proteasome system stress underlies synergistic killing of ovarian cancer cells by bortezomib and a novel HDAC6 inhibitor. Clin Cancer Res 2008;14:7340–7.
33. Martins FC, Santiago I, Trinh A, Xian J, Guo A, Sayal K, et al. Combined image and genomic analysis of high-grade serous ovarian cancer reveals PTEN loss as a common driver event and prognostic classifier. Genome Biol 2014;15:526.
34. Roh MH, Yassin Y, Miron A, Mehra KK, Mehrad M, Monte NM, et al. High-grade fimbrial-ovarian carcinomas are unified by altered p53, PTEN and PAX2 expression. Mod Pathol 2010;23:1316–24.
35. Tew WP, Sill M, McMeekin DS, Secord AA, Bonebrake AJ, Schilder J, et al. A randomized phase II trial of bevacizumab (BV) plus oral everolimus (EV) versus bevacizumab alone for recurrent or persistent epithelial ovarian (EOC), fallopian tube (FTC), or primary peritoneal cancer (PPC). 50th Annual Meeting of the American Society of Clinical Oncology (ASCO) Chicago, IL;2014.
36. Behbakht K, Sill MW, Darcy KM, Rubin SC, Mannel RS, Waggoner S, et al. Phase II trial of the mTOR inhibitor, temsirolimus and evaluation of circulating tumor cells and tumor biomarkers in persistent and recurrent epithelial ovarian and primary peritoneal malignancies: a Gynecologic Oncology Group study. Gynecol Oncol 2011;123:19–26.
37. Sarosiek KA, Cavallin LE, Bhatt S, Toomey NL, Natkunam Y, Blasini W, et al. Efficacy of bortezomib in a direct xenograft model of primary effusion lymphoma. PNAS 2010;107:13069–74.
38. Lee Y, Miron A, Drapkin R, Nucci MR, Medeiros F, Saleemuddin A, et al. A candidate precursor to serous carcinoma that originates in the distal fallopian tube. J Pathol 2007;211:26–35.
39. Pavelka N, Rancati G, Zhu J, Bradford WD, Saraf A, Florens L, et al. Aneuploidy confers quantitative proteome changes and phenotypic variation in budding yeast. Nature 2010;468:321–5.
40. Yang W, Soares J, Greninger P, Edelman EJ, Lightfoot H, Forbes S, et al. Genomics of drug sensitivity in cancer (GDSC): a resource for therapeutic biomarker discovery in cancer cells. Nucleic Acids Res 2013;41:D955–61.
41. Ohkawa K, Amasaki H, Terashima Y, Aizawa S, Ishikawa E. Clear cell carcinoma of the ovary: light and electron microscopic studies. Cancer 1977;40:3019–29.
42. Cochrane DR, Tessier-Cloutier B, Lawrence KM, Nazeran T, Karnezis AN, Salamanca C, et al. Clear cell and endometrioid carcinomas: are their differences attributable to distinct cells of origin? J Pathol 2017;243:26–36.
43. Jahn SC, Law ME, Corsino PE, Davis BJ, Harrison JK, Law BK. Signaling mechanisms that suppress the cytostatic actions of rapamycin. PLoS One 2014;9:e99927.

Downloaded from cancerres.aacrjournals.org on December 8, 2019. © 2019 American Association for Cancer Research.

Published OnlineFirst September 17, 2019; DOI: 10.1158/0008-5472.CAN-18-3029

Cancer Research
The Journal of Cancer Research (1916–1930) | The American Journal of Cancer (1931–1940)

AACR American Association for Cancer Research

Chromosomal Instability and mTORC1 Activation through PTEN Loss Contribute to Proteotoxic Stress in Ovarian Carcinoma

M. Herman Chui, Sasha A. Doodnauth, Natalie Erdmann, et al.

Cancer Res 2019;79:5536-5549. Published OnlineFirst September 17, 2019.

Updated version	Access the most recent version of this article at: doi:10.1158/0008-5472.CAN-18-3029
Supplementary Material	Access the most recent supplemental material at: http://cancerres.aacrjournals.org/content/suppl/2019/09/17/0008-5472.CAN-18-3029.DC1

Visual Overview	**A diagrammatic summary of the major findings and biological implications:** http://cancerres.aacrjournals.org/content/79/21/5536/F1.large.jpg

Cited articles	This article cites 42 articles, 10 of which you can access for free at: http://cancerres.aacrjournals.org/content/79/21/5536.full#ref-list-1

E-mail alerts	Sign up to receive free email-alerts related to this article or journal.
Reprints and Subscriptions	To order reprints of this article or to subscribe to the journal, contact the AACR Publications Department at pubs@aacr.org.
Permissions	To request permission to re-use all or part of this article, use this link http://cancerres.aacrjournals.org/content/79/21/5536. Click on "Request Permissions" which will take you to the Copyright Clearance Center's (CCC) Rightslink site.

Downloaded from cancerres.aacrjournals.org on December 8, 2019. © 2019 American Association for Cancer Research.